



OPEN ACCESS

EDITED BY

Ashish Rawson,
National Institute of Food Technology,
Entrepreneurship and Management,
Thanjavur (NIFTEM-T), India

REVIEWED BY

Maria Lidia Herrera,
University of Buenos Aires, Argentina
Prakyath Shetty,
National Institute of Food Technology,
Entrepreneurship and Management,
Thanjavur (NIFTEM-T), India

*CORRESPONDENCE

Wenhui Qi

✉ wenhui406@yeah.net

Zhisheng Zhang

✉ zhangzhisheng66@139.com

[†]These authors have contributed equally to this work

RECEIVED 16 November 2024

ACCEPTED 29 January 2025

PUBLISHED 19 February 2025

CITATION

Yang Q, Han P, Qi W, Shao Y, Zhang X, Wu F and Zhang Z (2025) High internal phase Pickering emulsion by ultrasound-modified almond protein isolate particles as a new fat substitute to improve oxidative stability of pork sausages.

Front. Sustain. Food Syst. 9:1529154.

doi: 10.3389/fsufs.2025.1529154

COPYRIGHT

© 2025 Yang, Han, Qi, Shao, Zhang, Wu and Zhang. This is an open-access article distributed under the terms of the [Creative Commons Attribution License \(CC BY\)](https://creativecommons.org/licenses/by/4.0/). The use, distribution or reproduction in other forums is permitted, provided the original author(s) and the copyright owner(s) are credited and that the original publication in this journal is cited, in accordance with accepted academic practice. No use, distribution or reproduction is permitted which does not comply with these terms.

High internal phase Pickering emulsion by ultrasound-modified almond protein isolate particles as a new fat substitute to improve oxidative stability of pork sausages

Qingrui Yang^{1†}, Peng Han^{2†}, Wenhui Qi^{1*}, Yutong Shao¹, Xu Zhang¹, Fengyang Wu¹ and Zhisheng Zhang^{1*}

¹College of Animal Science and Technology, Hebei Agricultural University, Baoding, China, ²Baoding Municipal People's Government, Baoding, China

Introduction: In this study, high-internal-phase Pickering emulsions (HIPPE) were used to produce low-fat meat products. The oxidative stability of HIPPE is a critical factor determining its suitability for this application.

Methods: Accordingly, an investigation was conducted to ascertain the impact of substituting 25–100% pig back fat with HIPPE (75% soybean oil, v/v) stabilized with ultrasound-modified almond isolate protein (UAPI) particles on the stability of sausages.

Results: The 300 W-UAPI sample exhibited the highest surface hydrophobicity value and emulsification activity index (87.65 m²/g), as well as the most optimal foaming stability (90.93%). Compared to the control emulsion, 300 W-UAPI-HIPPE exhibited the smallest average droplet size (30.49 μm), the highest oil loading ratio (82.26%), and improved antioxidant properties. The incorporation of UAPI-HIPPEs in sausages resulted in enhanced textural properties, including hardness, elasticity, chewiness, adhesion, and resilience, as well as increased densification. In addition, cooking loss and thiobarbituric acid-reactive substances content were reduced. Among the samples, those with 100% backfat substitution exhibited the most favorable textural properties and micromorphology, with a 67% reduction in cooking loss and the lowest fat oxidation.

Discussion: These findings indicate that UAPI-HIPPEs may serve as viable alternatives to animal fat in meat products, exhibiting desirable characteristics.

KEYWORDS

ultrasound, almond protein isolate, internal high phase Pickering emulsion, oxidative stability, sausage, texture

1 Introduction

High-internal-phase Pickering emulsions (HIPPEs) exhibit excellent rheological properties, are nontoxic, inexpensive, and are widely used in food, pharmaceutical, and cosmetic applications (Abdullah et al., 2020; Chen et al., 2018; Jiao et al., 2018; Shi et al., 2020). However, oil-in-water (O/W) HIPPEs are prone to oxidation, as the dispersed fat phase is over 74% (Zhu et al., 2024). The oil phase contains numerous unsaturated fatty acids, in which unsaturated fatty acids and oxygen interact to form hydroperoxides. Their decomposition products affect

the quality of many food products and cause nutrient loss. HIPPEs face oxidation as a major obstacle, urgent control or delay crucial. It has been demonstrated that the oxidation reaction of HIPPEs predominantly occurs at the oil–water interface. This encompasses the oxidation of lipids and solid particles attached to the periphery of oil droplets. Protein particles, which function as Pickering emulsifiers, can be used to impede lipid oxidation by scavenging free radicals, chelating pro-oxidative transition metals, or forming a physical barrier to segregate lipids from other active substances (Keramat et al., 2022).

The conformational relationship between the molecular structure of a protein and its physicochemical functional properties substantial affects the sensory properties of foods. Ultrasonication is a green, economical, and efficient method of protein modification. The cavitation effect of ultrasonication has been demonstrated to improve the structure of proteins (Rahman and Lamsal, 2021) while preserving their primary structure and nutrients. Zhou et al. (2021) stabilized HIPPE with quinoa protein particles produced using ultrasonication, and it is noteworthy that the physical and oxidative stability of the emulsion was enhanced by increasing the intensity of ultrasonication.

HIPPE, which was analogous to “black technology” in the food industry, could transform liquid oils into solid viscoelastic emulsion gels and had emerged as an alternative to saturated fats and hydrogenated oils in food components (Barth, 2007). β -lactoglobulin nanoparticle-stabilized HIPPE was used as an animal fat substitute in minced meat products, which markedly enhanced the hardness, elasticity, and chewiness of meat patties while inhibiting lipid oxidation (Villa et al., 2022). A substantial body of research has explored the potential of HIPPE as a substitute for animal fat. Nevertheless, only a few studies have documented the fabrication of HIPPEs using ultrasound-modified APIs, and even fewer studies have explored their utilization in meat products.

We constructed a stabilized O/W-type HIPPE, designated as UAPI-HIPPE, using an ultrasound-modified API (UAPI) as a solid particle emulsifier. This study aimed to investigate the potential of UAPI-HIPPE as a substitute for pig backfat in sausage production and validate its effect on oxidative stability in sausages. The structural and functional properties of the UAPI particles were characterized, and the microstructure of UAPI-HIPPE was examined using confocal laser scanning microscopy (CLSM) and scanning electron microscopy (SEM) to investigate the impact of UAPI particles on the stability of HIPPE. This approach was designed to establish a theoretical foundation for the application of UAPI-HIPPE as an alternative to animal fat in the food industry.

2 Materials and methods

2.1 Materials

Sweet almond meal was generously provided by Zhangjiakou Yong Chang Yuan Kernel Food Co. Ltd. (Zhangjiakou, Hebei, China). Soybean oil was purchased from the Huiyou Supermarket in Baoding, China. The reagents Nile Red, Nile Blue, and DPPH were purchased from Sigma-Aldrich (St. Louis, MO, United States). All other chemical reagents were purchased from Sinopharm Chemical Reagent Co Ltd. (Shanghai, China). Unless otherwise indicated, all experiments were conducted using deionized water.

2.2 Ultrasonic treatment of APIs

API was extracted from almond meal in accordance with the methodology outlined by Luo, with certain modifications (Luo et al., 2022). The resulting API content was approximately 912 g/1,000 g of powder with a nitrogen conversion factor of 6.25, as determined by the Kjeldahl method (Mandalari et al., 2010).

API suspensions (2%, w/v) (20 mL each) were poured into beakers (25 mL). Then, a Vibra-Cell TM ultrasonic processor (VC 750, Sonics & Materials, Inc., United States) fitted with a 13 mm diameter probe was used in the ultrasonic processing of API suspensions. API samples were subjected to ultrasound treatments (frequency 20 kHz, pulsed-mode duration of 3 s on and 3 s off for 2 min) for 150 W, 300 W, and 600 W, respectively. To prevent deterioration of the APIs owing to the excessive heat generated during sonication, the samples were maintained in an ice-water bath throughout the process. The untreated samples were used as controls. Subsequently, the pH of the suspension was adjusted to 2.5 with 1.0 M HCl, and stirred at 500 rad/min for 60 min at 25°C. The resulting protein suspension was freeze-dried. Samples were pre-cooled at -80°C for 2 h, lyophilized at -280°C for 48 h, and stored at 4°C until subsequent analysis.

2.3 HIPPEs preparation

A suspension solution of UAPI was prepared at a concentration of 2% with a pH of 2.5. The solution was then allowed to hydrate the protein suspension at 4°C for 24 h. A solution of the protein suspension (2 mL) was prepared by mixing it with 6 mL soybean oil. Subsequently, the mixtures were subjected to sonication using a high-intensity ultrasound processor (VCX-750, Sonics & Materials, Newton, CT) that fitted with a 13 mm diameter probe and 40% pressure amplitude for 10 s in a pulse mode (2 s on and 2 s off) in an ice-water bath. To prevent microbial growth during storage, sodium azide (0.2 mg/mL) was incorporated into the emulsion.

2.4 Preparation of pork sausage with HIPPEs

The sausage recipes were modified by replacing the pork backfat ratios with 300 W UAPI-HIPPEs loaded with astaxanthin, as illustrated in Table 1. Lean pork meat was cut into cubes and separately ground to the requisite sizes using a meat grinder. The ground lean minced meat, seasoning materials, and one-third pure water (4°C) were combined and chopped for 1 min. The ground backfat and one-third pure water (4°C) were then added and chopped for 1 min. Subsequently, the HIPPEs and the remaining water were incorporated and chopped for 1 min. The blended minced meat was then formed into sausages with a diameter of 2.5 cm. The sausages were tied with a string at 15-cm intervals, steamed, and stored at 4°C for subsequent analysis.

2.5 Characterization of APIs

2.5.1 Molecular mass

A sodium dodecyl sulfate–polyacrylamide gel electrophoresis (SDS-PAGE) was conducted with molecular weight markers ranging

TABLE 1 Ingredients composition of sausage processing.

Ingredients (%, w/w)	Treatment group				
	C	T1	T2	T3	T4
Lean pork	59.15	59.15	59.15	59.15	59.15
Pork backfat	24	18	12	6	–
Pure water	10	10	10	10	10
UAPI-HIPPE	–	6	12	18	24
Potato starch	4.5	4.5	4.5	4.5	4.5
Salt	1.3	1.3	1.3	1.3	1.3
Sodium ascorbate	0.03	0.03	0.03	0.03	0.03
Ginger powder	0.45	0.45	0.45	0.45	0.45
Five-spice powder	0.57	0.57	0.57	0.57	0.57
Total	100	100	100	100	100

C: The substitution ratio was 0; T1: The substitution ratio was 25%; T2: The substitution ratio was 50%; T3: The substitution ratio was 75%; T4: The substitution ratio was 100%.

from 10 to 180 kDa. The protein samples were observed to migrate at a constant voltage of 80 V at a slow rate into the concentrating gel. Upon reaching the 5% demarcation line of the concentrating gel and the 12.5% demarcation line of the separating gel, the voltage was increased to a constant value of 120 V until the bands extended to the bottom of the gel. Subsequently, the gel was stained with a staining solution [comprising Kaumas Brilliant Blue R-250 (0.2 g), 95% ethanol (84 mL), glacial acetic acid (20 mL), and water (200 mL)] for 2–3 h. Subsequently, the gel was destained with a destaining solution comprising 450 mL of 95% ethanol, 50 mL of glacial acetic acid, and 500 mL of water. Subsequently, the APIs were observed and photographed using a gel imager.

2.5.2 Secondary structure

Recording Fourier Transform Infrared Spectrometer (FT-IR) of ultrasound modified APIs using a spectrophotometer (FT-IR 8300 Shimadzu, Japan). The samples (10 mg) were mixed with KBr (200 mg) after drying to be grinded, and then pressed into thin slices. Absorption spectra was collected with the wave number range 400 cm^{-1} to 4,000 cm^{-1} at 25°C, the resolution was 4 cm^{-1} and the scanning frequency was 32 times. Graphical analysis was performed using Omnic 9.2 and Peakfit v 4.12 software.

2.5.3 Tertiary structure

The endogenous fluorescence spectra were determined using the method described by Tao et al. (2023), with certain modifications. The samples were diluted a specified number of times with deionized water under the following conditions: excitation at 280 nm, fixed slit width of 10.0 nm, scanning rate of 240 nm/min, and emission wavelength from 300 to 400 nm.

2.5.4 Surface hydrophobicity

The surface hydrophobicity of the API was estimated as the adsorption of bromophenol blue sodium salt (BPB), as described by Chelh et al. with slight modifications (Chelh et al., 2006). In particular, the absorbance of the sample solution treated with BPB was determined at 595 nm using a UV spectrophotometer to determine surface hydrophobicity.

2.5.5 Particle size

The particle sizes of the prepared APIs were analyzed using the Nano ZS90 (Malvern, Worcestershire, UK) and all samples were measured three times (Tian et al., 2020).

2.5.6 Scanning electron microscopy

SEM images of the APIs were obtained using a SEM (Thermo Fisher, United States) at an accelerating voltage of 30.0 kV and a magnification of 1,000 \times . The APIs were affixed to a metal stand with a conductive adhesive and coated with gold before testing.

2.5.7 Emulsifying properties of APIs

The emulsification activity index (EAI) and emulsification stability index (ESI) are two key parameters used to assess the stability and consistency of emulsions. A mixed API solution (10 mg/mL) with soybean oil in a volume ratio of 7:3 was subjected to treatment with a centrifugal force of 11,180 g for 1 min. Following the emulsification process, 50 μL was rapidly absorbed from the base of the emulsions and then vortex-mixed with a 15 mL solution of 0.1% sodium dodecyl sulfate. The absorbance was measured at 500 nm using a spectrophotometer at both the initial time point (0 min) and the subsequent time point (10 min). The calculation formula is as follows (Equations 1–2):

$$\text{EAI} = 2T \times \frac{A_0 \times N}{\varphi \times L \times C \times 10000} \quad (1)$$

$$\text{ESI} = \frac{A_{10} \times 100}{A_0} \quad (2)$$

N represents the dilution factor of 100, L denotes the light path of 1 cm in the colorimetric cell, T is a constant of 2.303, the volume fraction of the oil phase is 30%, C is the initial protein concentration of 10 mg/mL, and A_0 and A_{10} are the absorbance values of the emulsion at 0 min and 10 min, respectively.

The foaming index (FC) and foaming stability index (FS) are calculated as follows (Equations 3–4): The methodology described by Tian et al. (2020) was adapted with minor modifications. To prepare a solution of 100 mL at a concentration of 10 mg/mL, the pH value was adjusted, mixed at 8,000 rpm for 2 min through a high-speed disperser, and immediately transferred to a 500 mL measuring cylinder. The homogenizer's interior surface was rinsed with minimal distilled water, and the foam volume was measured after mixing stopped. The total volumes of liquid and foam were recorded at 30, 60, and 90 min.

$$\text{FC} = \frac{V_1 - V_0}{V_0} \times 100\% \quad (3)$$

$$\text{FS} = \frac{V_2 - V_0}{V_0} \times 100\% \quad (4)$$

where V_0 is the sample volume (mL), V_1 is the total volume of liquid and foam when stirring stopped (mL), and V_2 is the total volume of liquid and foam after 30 min, 60 min, and 90 min (mL).

2.6 Characterization of HIPPEs

2.6.1 Microstructure observation

The microstructures of the fresh HIPPEs were evaluated using a Carl Zeiss LSM800, as previously described by [Chen et al. \(2023\)](#). In summary, 20 μL of a mixed fluorescent fuel (comprising 10 μL of 0.2% Nile Red and 10 μL of 0.2% Nile Blue) was added to fresh HIPPEs (1 mL), which were then incubated in the dark for 20 min. Subsequently, the stained HIPPEs (10 μL) were added to a glass slide and imaged using a 40 \times objective lens. Excitation wavelengths of 488 and 633 nm were used, emission wavelengths of 519 nm and 660 nm, respectively.

2.6.2 Measurement of droplet size

The droplet size was measured using the method described by [Deng et al. \(2021\)](#) with slight modifications. The fresh HIPPEs were diluted 1,000-fold for detection by Nano ZS90 at 25°C. The data were reported as Z-average size. Measurements were conducted in triplicate and repeated thrice for each sample.

2.6.3 Interface adsorption rate of proteins

The protein adsorption rate was determined according to the methodology described by Zhang et al. with some modifications ([Zhang et al., 2020](#)). Eight milliliters of freshly prepared HIPPEs were subjected to centrifugation force of 11,180 g for 1 min at 4°C. The lower aqueous phase was collected using a syringe, and the protein content was determined using Lowry's reagent. The percentage of adsorbed proteins was then determined.

2.6.4 Determination of lipid oxidation and protein oxidation in HIPPEs

To assess the oxidation stability of the HIPPEs in accordance with the established methodology, the samples were placed in small glass vials with tightly screwed caps and incubated for 14 days in the dark at 37°C. Lipid content was quantified by monitoring alterations in hydroperoxide and 2-thiobarbituric acid reactive substances (TBARS) ([Shantha and Decker, 1994](#)). The extent of protein oxidation was determined by analysing the protein carbonyl and free sulfhydryl content ([Marquez et al., 2010](#)).

Hydroperoxides: One gram of emulsion was combined with 5 mL of iso-octane:isopropanol (2:1, v/v) reagent, vortexed for 30 s, and centrifuged at 5,000 rpm for 5 min. One hundred microliters of the resulting supernatant were then combined with 40 μL of ferrous solution (equal parts of 0.132 mol/L barium chloride and 0.144 mol/L ferrous sulfate) and 40 mL of 3.94 mol/L ammonium thiocyanate solution. Following a 20-min reaction period in the absence of light, the absorbance value was determined at 510 nm using an enzyme meter. A standard curve was prepared using a hydrogen peroxide standard solution at a concentration of 1,000 $\mu\text{g}/\text{mL}$.

TBARS solution was prepared by mixing TCA and 0.10% EDTA, vortexing for 30 s, and filtering. A volume of 2.50 mL of the filtrate was pipetted and heated in boiling water for 40 min with the addition of 0.02 mol/L TBA. After cooling, 5.00 mL CHCl_3 was added, vortexed, and mixed thoroughly. Centrifugation was performed to collect the supernatant. The absorbance at 532 nm was measured using a spectrophotometer.

Carbonyl content was determined by the following procedure: A solution of 0.2 mL of emulsion was prepared by mixing with 0.8 mL of 2 mol/L HCl (containing 10 mmol/L DNPH). A blank control

solution of 2 mol/L HCl without DNPH was also prepared. The reaction was performed for 1 h at room temperature. After completion of the reaction, 0.4 mL of trichloroacetic acid (TCA, 40%) was added, and the mixture was left to stand at room temperature for 0.5 h. The precipitate was separated using 1 mL ethanol/ethyl acetate. Following a one-hour reaction period, 0.4 mL of trichloroacetic acid (TCA, 40% by mass) was added, mixed thoroughly, and left to stand for an additional 0.5 h. Centrifugation at 8,000 rpm for 10 min at 4°C was performed, after which the supernatant was removed. The precipitate was subsequently washed three times with 1 mL ethanol/ethyl acetate (1:1, v/v). Subsequently, the precipitate was dissolved in 1.0 mL of 0.02 mol/L phosphate buffer (pH 6.5, containing 6 mol/L guanidine hydrochloride), and the absorbance at 370 nm was measured to calculate the carbonyl content.

Free sulfhydryl content was determined using the method described by Ellman et al. mL of the emulsion was combined with 2.0 mL of the 0.03 g/mL SDS solution, followed by the addition of 0.2 mL of DTNB solution (0.5 mL), which could react in the presence of light for approximately 1 h. The absorbance was measured at 412 nm. The control group comprised samples lacking DTNB solution, and the protein content was determined using a bicinchoninic acid kit. Subsequently, sulfhydryl content was determined ([Equation 5](#)).

$$\text{SH (nmol / mg protein)} = \frac{73.53 \times A_{412} \times D}{C} \quad (5)$$

Where A_{412} is the absorbance of the sample after removal of the control (73.53), is the conversion factor, D is the dilution factor, and C is the protein concentration (mg/mL) in the sample.

2.7 Characterization of pork sausage

2.7.1 Scanning electron microscopy of sausages

The microstructure of the sausages was observed via SEM using the methodology outlined by [Xia et al. \(2019\)](#) with minor modifications. The freeze-dried samples were affixed to metal trays with conductive double-sided tape and the surfaces were coated with a thin layer of gold powder to prevent charging under the electron beam. Subsequently, the samples were observed using a Prisma E scanning electron microscope (Thermo Fisher Scientific, United States) at an accelerating voltage of 30.0 kV, and images were captured.

2.7.2 Cooking loss of sausage

Cooking loss of the sausages was quantified according to the methodology outlined by [Choe et al. \(2013\)](#). Three sausages were used for each treatment batch. Raw sausages were weighed and subsequently cooked for 30 min at 80°C. After cooling for 1 h, the sausages were gently wiped, cooled to room temperature, and weighed again. Cooking loss was calculated by repeating the process three times in parallel for each sample as follows ([Equation 6](#)):

$$\text{Cooking loss (\%)} = \frac{\text{Weight before heating} - \text{Weight after heating}}{\text{Weight before heating}} \times 100\% \quad (6)$$

2.7.3 Texture profile analysis of sausage

The texture of the sausages was evaluated according to the methodology proposed by Li et al. (2023). The sausages were stripped of their casings and cut into cylinders with a height of 20 mm and a diameter of 20 mm. Six segments were selected from each group of samples to determine the relevant textural parameters, which were analyzed using a physical property analyzer (TPA). The measured parameters were a post-test speed of 1 mm/s, compression ratio of 70%, and trigger force of 5 g. A 50 mm aluminum cylinder was used as the probe.

2.7.4 Determination of fat oxidation

The rate of fat oxidation was determined by measuring the concentration of TBARS according to the method of Wang and Xiong, with minor modifications (Wang and Xiong, 2005). The prepared sausages were stored in a refrigerator at 4°C, and the TBARS content was determined on days 1, 2, 3, 4, 5, 6, and 7. A 2-g sample of chopped sausage was combined with 8.5 mL of 2.5% trichloroacetic acid solution (dissolved in 36 mmol/L hydrochloric acid solution). A 5-mL sample of a 1% 2-thiobarbituric acid (TBA) solution (prepared by dissolving the compound in a 75 mmol/L sodium hydroxide solution) was boiled for 30 min. The resulting supernatant (5 mL) was cooled to room temperature and mixed with an equal volume of chloroform. The mixture was subsequently centrifuged at 2,000 × g for 10 min. The supernatant (5 mL) was cooled to room temperature, mixed with an equal volume of chloroform, and centrifuged for 10 min at 2,000 × g. The absorbance of the mixture was measured at a wavelength of 532 nm. TBARS values were expressed as milligrams of malondialdehyde per kilogram of sample (mg MDA/kg) and calculated according to the following formula (Equation 7):

$$\text{TBARS (mg / MDA / Kg)} = \frac{A_{532}}{M_s} \times 9.48 \quad (7)$$

where A_{532} is the absorbance at 532 nm, M_s is the weight of the sausage sample (g), and 9.48 is the dilution factor and molar extinction coefficient ($152,000 \text{ M}^{-1} \text{ cm}^{-1}$) derived from the red TBA reaction product constant.

2.8 Statistical analysis

Statistical analyses were conducted using the statistical software packages SPSS 26.0 and Origin 2021 (United States). Variability between samples was determined using Duncan's method of comparison, with a significance level of $p < 0.05$.

3 Results and discussion

3.1 Characterization of APIs

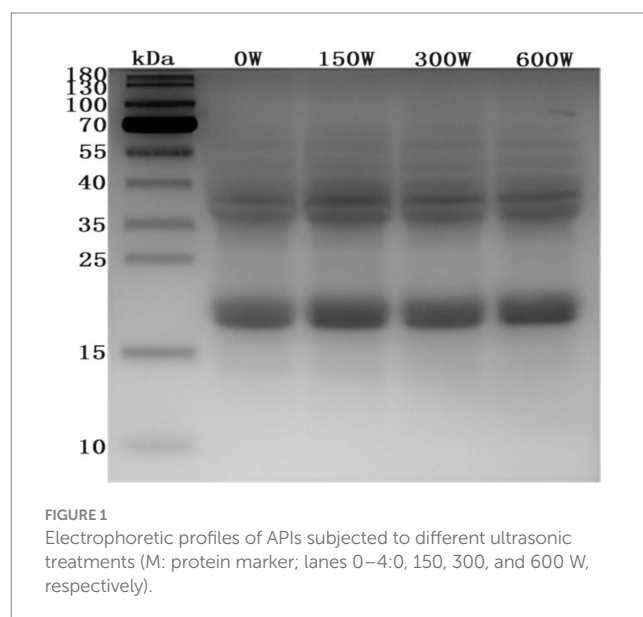
3.1.1 Primary structure

The impact of the ultrasonically modified API was evaluated using SDS-PAGE. Electropherograms demonstrated that the molecular weight of the hydrophilic almond protein was within the range of 20–70 kDa (Figure 1), predominantly comprising two subunit groups of 18–22 kDa and 36–38 kDa, respectively. Furthermore,

electropherograms showed that there were no notable discrepancies in the molecular weights of the samples. This indicates that the chemical bonds within the protein molecules remained intact. This suggests that ultrasound treatment did not provide sufficient energy to alter the primary structure of APIs (Jiang et al., 2023).

3.1.2 Secondary structure

Figure 2 illustrates the impact of sonication on the Fourier Transform Infrared Spectroscopy (FTIR) spectrum (A) and the secondary structure (B) of API. The amide I band ($1,700\text{--}1,600 \text{ cm}^{-1}$) is commonly employed to analyze the secondary structure of proteins. This band predominantly represents the C=O stretching vibration of the amide group, along with in-plane N-H bending and C-N stretching (Herrero, 2008). The α -helices are stabilized primarily by hydrogen bonds formed between the carbonyl oxygen (C=O) and the amino hydrogen (N-H) of the molecule (Martinez et al., 2020). As shown in Figure 2A, characteristic absorption peaks of the FTIR spectra are observed in the $800\text{--}1,800 \text{ cm}^{-1}$ range following different treatments. Through Gaussian fitting and peak area analysis, the secondary structure content of the amide I band was quantified, as displayed in Figure 2B. With increasing ultrasonic power (0–600 W), the α -helix content decreased from 28.3 to 14.3%, while β -sheet content rose from 7.4 to 14.9%. Concurrently, β -turn and random coil content increased from 19.9 and 44.4% to 23.9 and 47.6%, respectively. These results suggest that sonication cleaves hydrogen bonds within API and facilitates the reorganization of peptide chains. A previous study reported that the reduction in α -helices and an increase in β -sheets exposes hydrophobic regions in proteins, enhancing hydrophobicity and altering their processing properties (Li et al., 2023). Ultrasonic cavitation generates strong hydrodynamic shear, localized high temperatures, and high pressure, which disrupt the secondary structure of proteins. This disruption promotes the transformation of α -helices into β -turns and β -sheets, leading to protein unfolding and dissociation of the native conformation. Such structural disorder increases the surface activity and emulsification capacity of the protein compared to ordered structures (Li et al., 2019). These findings align with the results of surface hydrophobicity analysis.



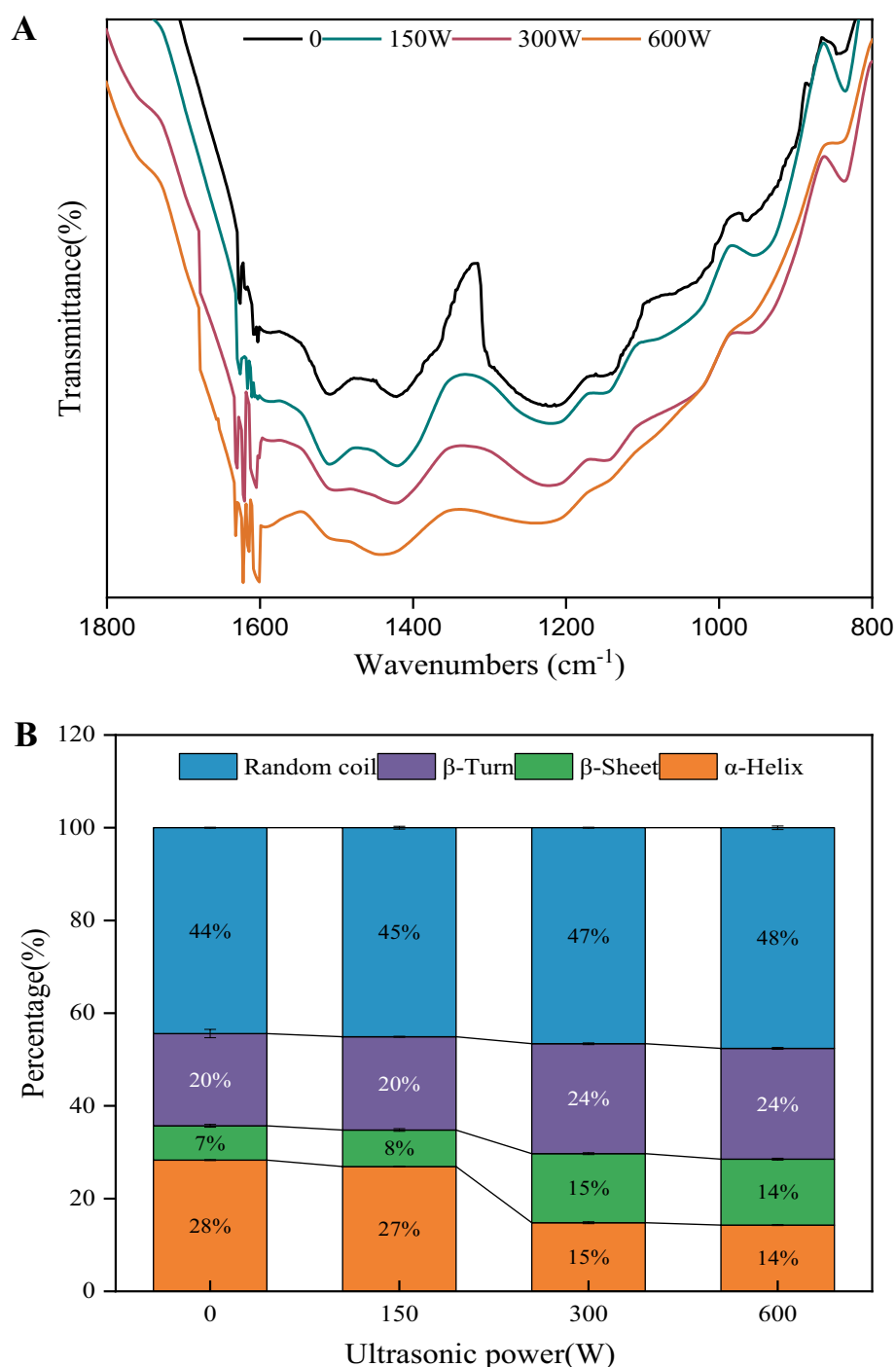


FIGURE 2 Fourier transform infrared spectroscopy (A) and protein secondary structure (B) of the ultrasound-modified API.

3.1.3 Tertiary structure

The tertiary structure of proteins is reflected by changes in the fluorescence intensity of aromatic amino acid residues (Tao et al., 2023). Endogenous fluorescence spectra in the tertiary structure of the ultrasonic-modified API were used to elucidate these changes, and the resulting experimental data are presented in Figure 3. Prior research has demonstrated a correlation between fluorescence intensity and the quantity of aromatic amino acids present within a protein molecule or near nonpolar amino acids. Compared to unmodified APIs, the

fluorescence intensity of ultrasound-modified APIs increased. The application of an appropriate ultrasonic power can facilitate the separation of protein structures and exposure of aromatic amino acid residues, inducing a red shift in the endogenous fluorescence spectrum. The maximum wavelength of emission exhibited a red shift from 342.2 nm to 332.4 nm in 300 W, indicative of a rearrangement in the tertiary structure to enhance the surface hydrophobicity of proteins. However, the endogenous fluorescence spectrum of almond protein exhibited a blue shift at an ultrasound power of 600 W. This suggests

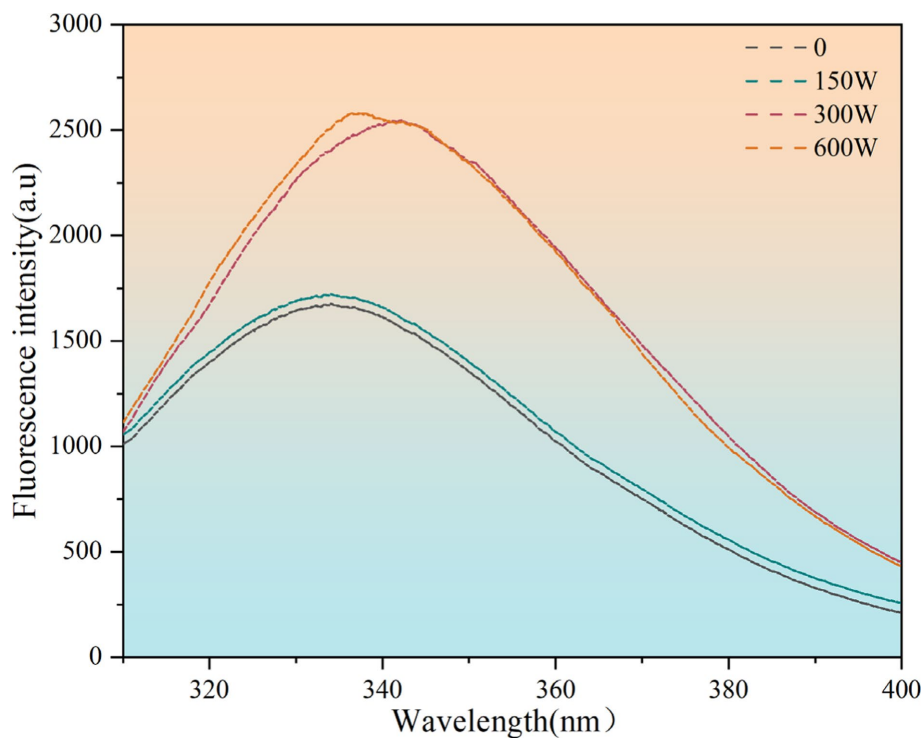


FIGURE 3
Intrinsic fluorescence spectrum of the ultrasound-modified API.

that appropriate ultrasonic treatment can enhance the degree of protein structure unfolding and inhibit the mutual aggregation phenomenon between proteins, which lead to increased protein oxidation, enhanced aggregation, and a blue shift. This result is consistent with the findings of Deng et al., who observed that ultrasonic treatment altered the tertiary structure of myofibrillar fibrillar proteins isolated from the new silverfish *Mytilus edulis* in Taihu Lake, enhancing their functional characteristics (Deng et al., 2021).

3.1.4 SEM of UAPI

Figure 4 depicts the microstructural images of the ultrasound-modified proteins observed via SEM at 10,000 \times magnification. Compared with the API that had not undergone ultrasonic treatment, the protein structure that had been treated ultrasonically exhibited severe fracturing with visible pores, particularly at 600 W. It was demonstrated that the magnitude of ultrasonic power significantly affected the structure of the APIs. Sun et al. (2022) observed the effect of ultrasound on protein structure, whereas Tian et al. (2020) noted that ultrasonic treatment altered the structure of soybean proteins. The alteration in the protein structure can also be attributed to the unfolding of the protein structure due to the turbulence and microcurrents generated by ultrasonication, which breaks down the protein structure from a macromolecular structure to a small subunit structure and increases the contact area between the protein particles and water. This may explain the increase in solubility observed after ultrasonication.

3.1.5 Surface hydrophobicity

Hydrophobic properties of protein surfaces are a key indicator of conformational changes, as protein folding is primarily driven by

hydrophobic interactions (Oliete et al., 2018). Surface hydrophobicity reflects alterations in the number and distribution of hydrophobic groups on the protein surface and can be assessed by the binding strength of bromophenol blue to the protein (Jia et al., 2017). As shown in Table 2, the surface hydrophobicity of API particles increased with rising sonication power from 0 to 600 W. This increase is attributed to the mechanical forces generated by ultrasonic cavitation, which disrupted intermolecular interactions, causing the API structure to unfold and exposing nonpolar, hydrophobic amino acids such as methionine, phenylalanine, and tryptophan (Hu et al., 2013). Similar observations have been reported in studies on quinoa (Qin et al., 2018), silkworm pupae (Jiang et al., 2023) and oat proteins (Li and Xiong, 2021). The maximum surface hydrophobicity was observed at a sonication power of 300 W (21.92), significantly higher than the untreated control API particles (14.82, $p < 0.05$). This enhancement in surface hydrophobicity suggests that appropriate ultrasonic treatment promotes the exposure of API hydrophobic groups (Ji et al., 2015). However, at a higher sonication power of 600 W, surface hydrophobicity decreased. This decline is likely due to excessive hydrophobic interactions between particles, resulting in the formation of insoluble aggregates and a consequent reduction in protein surface hydrophobicity (Cao et al., 2021).

3.1.6 Particle size

Figure 5 illustrates the significant reduction in the average particle size of UAPI following ultrasonic treatment. Specifically, the particle size decreased from 489.77 nm for un-sonicated API to 297.90 nm at an ultrasonic power of 600 W. This reduction can be attributed to the breakdown of larger insoluble peptide aggregates by cavitation, turbulent forces, and microfluidic effects generated during ultrasonic

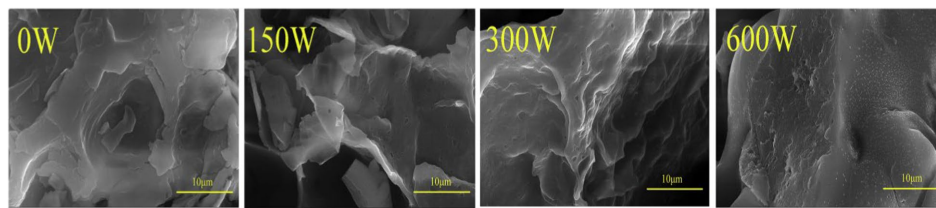


FIGURE 4
Scanning electron microscope image of the ultrasonically treated API (magnification 1,000×).

TABLE 2 Emulsification performance indicators for ultrasonically treated APIs.

Ultrasonic power (W)	Surface hydrophobicity index (μg)	EAI (m^2/g)	ESI (min)	FC (%)	FS (%)		
					30 min	60 min	90 min
0	14.82 ± 0.86^a	78.15 ± 0.95^a	94.40 ± 0.26^a	84.97 ± 0.65^a	83.80 ± 0.75^a	34.97 ± 0.64^a	9.63 ± 1.29^a
150	17.98 ± 0.30^b	79.16 ± 0.27^a	94.71 ± 0.41^a	86.60 ± 0.17^b	85.37 ± 0.23^b	46.60 ± 0.17^b	13.70 ± 0.70^b
300	21.92 ± 1.49^c	87.65 ± 0.42^c	97.55 ± 0.44^b	90.93 ± 0.45^d	90.57 ± 0.58^d	80.93 ± 0.41^d	21.33 ± 0.72^c
600	18.72 ± 1.40^b	84.41 ± 0.38^b	94.36 ± 0.56^a	87.47 ± 0.15^c	86.47 ± 0.15^c	67.47 ± 0.15^c	13.53 ± 0.31^b

Letters a–d in the same column represent significant differences in data in the same column ($p < 0.05$).

treatment (Morales et al., 2015). Additionally, ultrasonic vibrations may cause violent collisions between protein molecules, resulting in the formation of smaller protein particles (Gulseren et al., 2007). Several studies have demonstrated the effectiveness of ultrasound in reducing particle size. For example, Jiang et al. (2023) reported a reduction in the average particle size of silkworm chrysalis protein from 2869.33 nm to 314.30 nm after ultrasonic treatment at a power output of 520 W for 10 min. Similar results have been observed for the ultrasonic treatment of quinoa protein (Zhang et al., 2021) and rice protein (Zhang et al., 2021).

3.1.7 Emulsifying properties of API

The emulsifying nature of solid particles is a determining factor in their ability to form oil–water interface films and their resistance to deformation. The effects of ultrasound on the EAI and ESI of APIs are shown in Table 2. The EAI value of 300 W-UAPI was the highest ($87.65 \text{ m}^2/\text{g}$), representing a 12.16% increase compared to the control APIs. The cavitation effect of ultrasound changes the tertiary structure of API particles and breaks the hydrogen bonds of the molecular structure, resulting in a smaller volume of API, which accelerates the migration and diffusion of API to the oil–water interface. Increased surface hydrophobicity promotes interactions between protein particles in the interfacial layer, improving the tightness of the interfacial layer and the stability of the emulsion. The ESI value of the 300 W-UAPI was the highest (97.55 min), representing a 3.34% increase over the control API. A previous study reported that the EAI and ESI of peanut meal protein improved after ultrasonic treatment (Chen and Zhang, 2023). However, the ESI index of UAPI decreased for 600 W, which was attributed to the hydrophobic interactions of proteins accelerating protein aggregation. Thus, particle size and surface hydrophobicity were key factors in determining the emulsification performance of API particles.

Table 2 illustrates the impact of ultrasonication on the FC and FS indices of APIs. The control group exhibited the lowest FC index (84.97%). The FC index of the 300 W-UAPI-HIPPEs was the highest

(90.93%), representing a 7.01% increase compared to the control group. Ultrasonication caused the exposure of additional hydrophobic groups in the API molecules, enhancing their surface activity. This enabled the APIs to fully unfold at the gas–liquid interface, with continuous phase wrapping around the air to form substantial foam during the ultrasonication process. Following sonication, the number of hydrophobic groups exposed on the surface of the API molecules increased, the surface activity was enhanced, the API was fully unfolded at the gas–liquid interface, and numerous bubbles were formed by wrapping air in the continuous phase during the sonication process. Following a 30-min period of standing period, the FS index of 300 W-UAPI exhibited minimal change. This may be attributed to the rapid adsorption of API onto the air–water interface, which was then subjected to molecular rearrangement. This resulted in the polar groups unfolding toward water and the hydrophobic groups stretching out toward air, forming a viscoelastic thin film at the interface. This process led to a rapid decrease in the surface tension and an increase in the foam stability. Asif et al. (2024) used ultrasound treatment of moringa seed protein and discovered that ultrasound treatment enhanced the foam stability index of moringa seed protein.

3.2 Characterization of HIPPEs

3.2.1 Microstructure of HIPPEs

The microstructures of the HIPPEs were characterized by CLSM. As illustrated in Figure 6, CLSM demonstrated that soybean oil droplets labeled with Nile Red (red) were encased by API or UAPI labeled with Nile blue (green), indicating that O/W HIPPE could be formed using API or UAPI at pH 2.5. The successful adsorption of API or UAPI on the oil–water interface results in the formation of a physical barrier around the periphery of the oil droplets, preventing droplet coalescence. A comparable phenomenon has been observed in HIPPEs stabilized by composite nanoparticles formed by

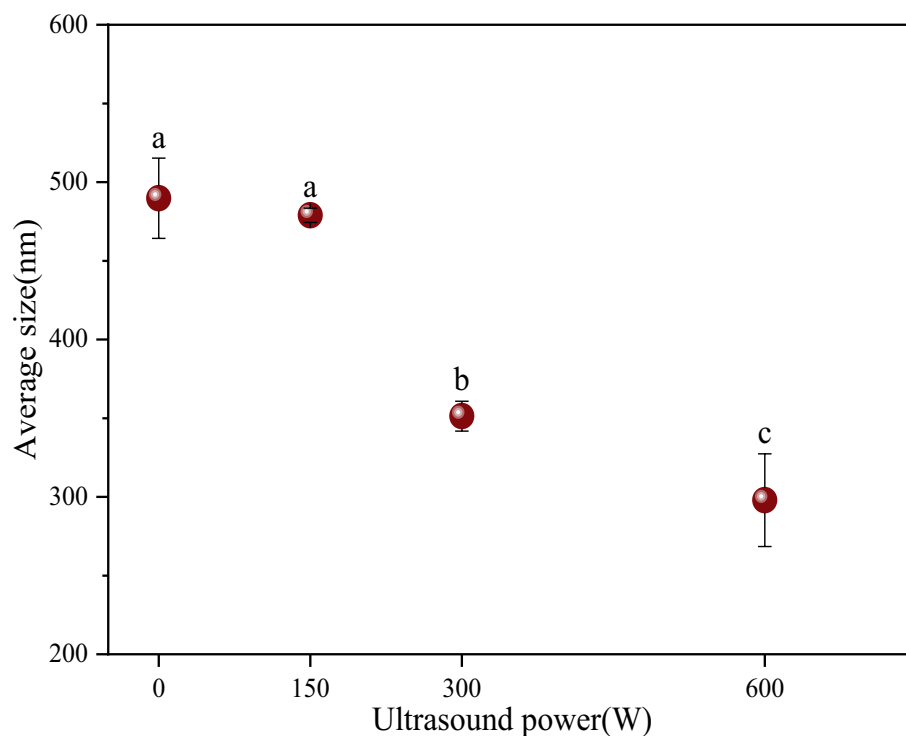


FIGURE 5
Particle size distribution of API treated with 0–600 W ultrasonic power at pH2.5.

alcohol-soluble proteins (Zhang et al., 2020) or soy protein- β -glucan catechin complex nanoparticles (Chen et al., 2023).

3.2.2 Droplet size

Droplet size is the principal criterion used to assess the physicochemical stability of HIPPE. The measurements of fresh HIPPE droplet size are shown in Figure 7. A comparison of the droplet size in the UAPI-HIPPE group with that in the control group revealed a significant reduction ($p < 0.05$). The 300 W-UAPI-HIPPE exhibited the smallest droplet size of 30.49 μm , indicating that the ultrasonic treatment facilitated API adhesion to the emulsion-water-oil interface, enhanced interfacial protein adsorption capacity, and formed a dense 3D network interfacial barrier, improving the physical stability of HIPPE. Similarly, Ma et al. reported that ultrasonic treatment improved the physical and chemical properties of cod protein, formed smaller droplets, and improved the stability of oil-water emulsions (Ma et al., 2019). Deng et al. reported that high-intensity ultrasound promoted the formation of small droplets on serpentine myofibrillar proteins and significantly improved the oxidative stability of emulsions (Deng et al., 2021).

3.2.3 Interface protein adsorption rate and fuel loading rate

Figure 8 illustrates the impact of the US-modified API on the interfacial adsorption of proteins in the high-phase emulsions. The interfacial protein adsorption rates of the 150 W-UAPI-HIPPEs and 300 and 600 W-UAPI-HIPPEs were 40.68, 47.69, and 46.49%, respectively, which were significantly higher than those of the control (37.38%). The observed increase in the interfacial protein adsorption rate can be attributed to a reduction in the particle size and an

enhancement in the surface hydrophobicity of the APIs following sonication. The smaller proteins exhibited enhanced diffusion rates to the oil droplet surface, facilitating the reduction of the interfacial tension. Ultrasonic treatment facilitates the adsorption of greater quantities of proteins at the oil-water interface and the formation of protein films at the emulsion interface (Peng et al., 2016). This was attributed to the improvement in the flexible structure of the proteins by ultrasonic treatment (Yan et al., 2021), which enlarged the spatial structure of the proteins and exposed the hydrophobic groups. The emulsion droplets exhibited a reduction in the particle size and an increase in the interfacial specific surface area. The interfacial protein adsorption rate increased, forming a physical barrier around the droplet periphery. The surplus API in the aqueous phase undergo cross-linking, which further reinforces the 3D network structure of the emulsion, more effectively securing the oil droplets, preventing their agglomeration, and enhancing the oil-carrying capacity of the emulsion system. The maximum internal comparison of 300 W-UAPI-HIPPE was 82.26%, which was 1.95% higher than the control.

3.2.4 Lipid oxidation in HIPPEs

Lipid oxidation was investigated by monitoring the generation of primary (lipid hydroperoxides) and secondary reaction products (thiobarbituric acid reactive substances, TBARS) during 14 days of storage at 37°C (Figure 9). In all emulsions, both primary and secondary products accumulated progressively during storage, indicating that lipid oxidation occurred. As illustrated in Figure 7, the hydroperoxide levels of both UAPI-HIPPEs were significantly lower during storage than those in the control. The fresh control sample exhibited a hydroperoxide value of approximately 0.05 mmol/L, which increased to 0.38 mmol/L by day 14, representing a 6.6-fold increase

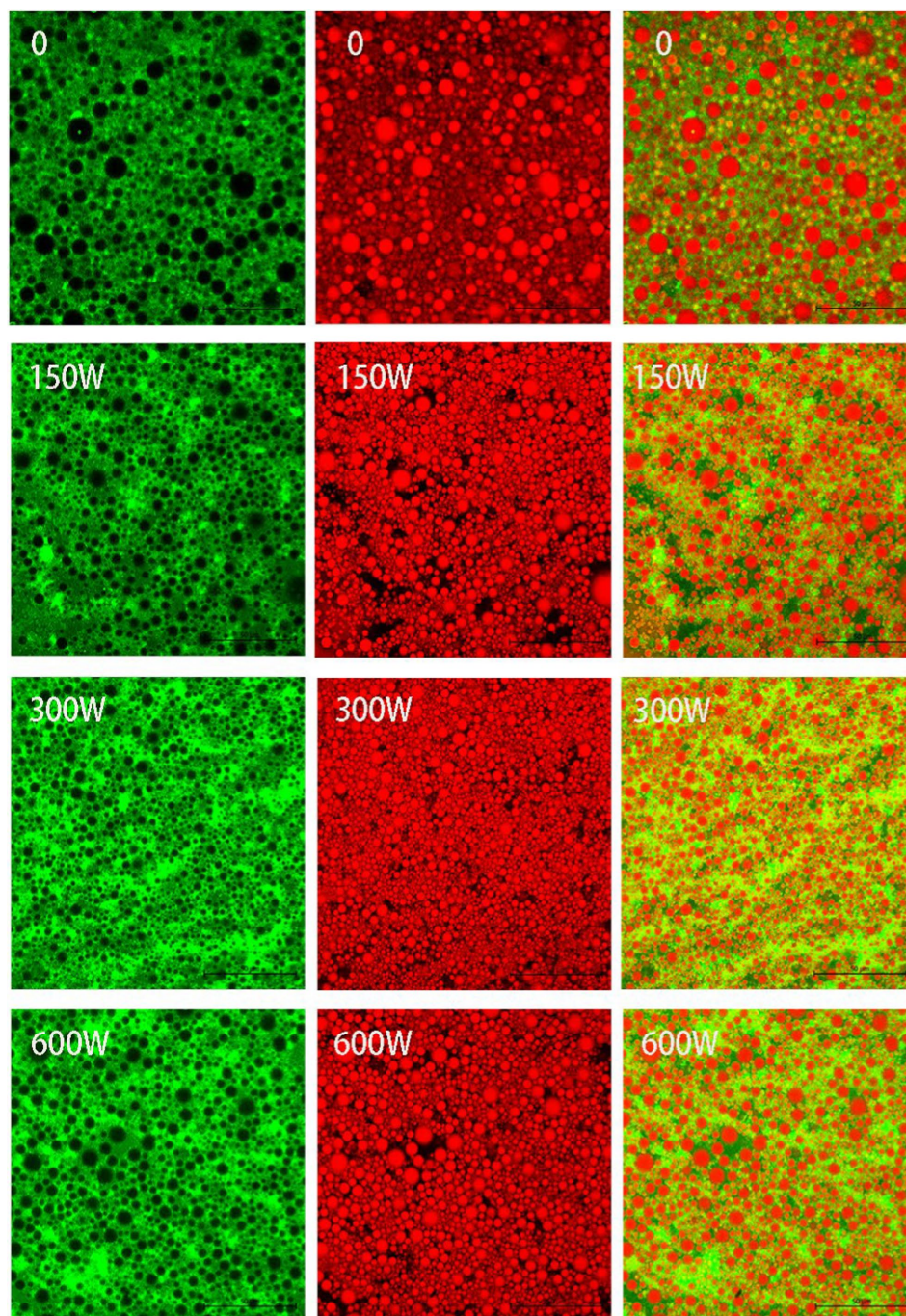


FIGURE 6
Confocal laser scanning images of UAPI-HIPPEs.

($p < 0.05$). In contrast, the emulsions prepared from sonicated APIs exhibited significantly reduced hydroperoxide levels compared those with of the control. The hydroperoxide yield of 300 W-UAPI-HIPPE was as low as 0.22 mmol/L on day 14, a 4.6-fold increase, which was significantly lower than that of the control group ($p < 0.05$). UAPI, which has excellent adsorptive properties (as shown in Figure 8), migrated rapidly to the oil–water interface, forming a thick three-dimensional network barrier that partially blocked the oxidative (Zhang et al., 2021). It is noteworthy that the trend of TBARS in emulsions is similar to the trend of hydroperoxide values. Previous

studies on proteins have shown that non-adsorbed proteins can bind pre-oxidants (e.g., transition metal ions) and therefore inhibit their ability to adsorb to the droplet surface and promote oxidation (Gumus et al., 2017).

The results indicate that ultrasound-modified API has better interface antioxidant activity than that of the control sample, which may be due to the inherent antioxidant activity of ultrasound-modified API molecules, including free radical scavenging and chelation of ferrous ions (Joshi et al., 2013). Ultrasound-modified proteins improve the oxidative stability of emulsions because they are

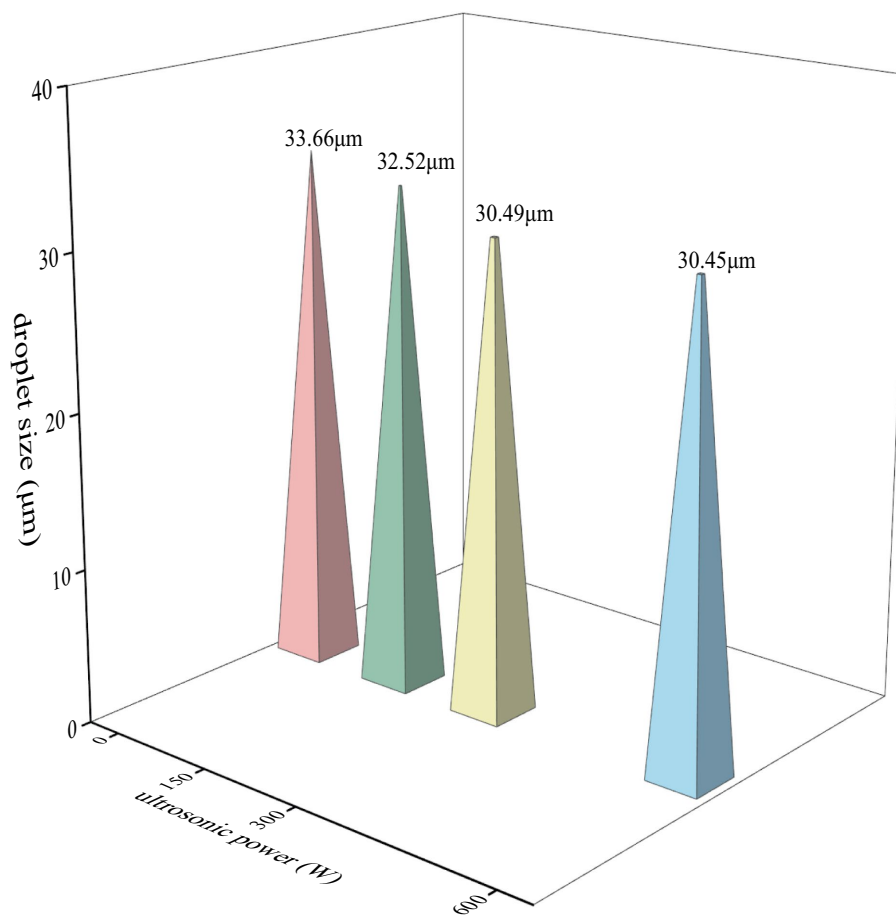


FIGURE 7
Droplet size of UAPI-HIPPEs.

able to form thicker coatings around oil droplets, spatially inhibiting water-soluble pro-oxidants from reaching emulsified lipids. For example, ultrasonic-modified quinoa protein (Schroen and Berton-Carabin, 2022) and ultrasonic-modified silkworm pupa protein (Jiang et al., 2023) were found to improve the antioxidant stability of emulsions.

3.2.5 Protein oxidation in HIPPEs

Protein (e.g., hemp seed protein and α -lactalbumin) particles can act as antioxidants in the continuous phase of oil-in-water emulsions (Li et al., 2022; Qayum et al., 2021). Carbonyl formation is one of the first stages of protein oxidation; therefore, the carbonyl content in emulsions was determined to evaluate the degree of oxidative damage to proteins (Berton et al., 2012). As shown in Figure 10, the total carbonyl content in the emulsions of all treatment groups increased gradually during 14 days of storage, indicating that protein oxidation occurs due to secondary reactions between lipid oxidation products and amino acid side chains. However, the carbonyl concentration of 300 W-UAPI-HIPPE was the lowest on day 14 (13.25 $\mu\text{mol/kg}$), and this value was significantly lower than that of the control ($p < 0.05$).

As shown in Figure 10, the sulfhydryl content of all emulsions showed a decreasing trend during storage, and the rate of sulfhydryl formation in UAPI-HIPPEs was significantly lower than that in the control group, suggesting that UAPI inhibits protein oxidation due to

the formation of cross-links between protein sulfhydryl groups and interactions between the exposed sulfhydryl groups and other compounds, which leads to a decrease in sulfhydryl content. On the 14th day, the sulfhydryl content of the 150 W-UAPI-HIPPE, 300 W-UAPI-HIPPE, and 600 W-UAPI-HIPPE groups was 441.19 $\mu\text{mol/g}$ protein, 455.12 $\mu\text{mol/g}$ protein, 487.47 $\mu\text{mol/g}$ protein, and 460.72 $\mu\text{mol/g}$ protein, respectively. These values were 0.89, 10.49, and 4.43% higher than those in the control group, respectively. Sonication decreased the overall hydrophobicity of the API protein surface, which led to a decrease in the production of carbonyl groups; the increase in hydrophobicity helps to stabilize the protein structure and reduces the likelihood of oxidation reactions and the production of oxidation products (Sun et al., 2022). In addition, the reduced production of lipid oxidation products in emulsions containing ultrasound-modified APIs may have reduced the rate of protein oxidation due to the exposure of the hydrophobic groups.

3.3 Characterization of sausages

3.3.1 The appearance and structure of sausages

Figure 11 illustrates the microstructures of sausages produced with varying ratios of UAPI-HIPPE instead of pig backfat. The sausages exhibited irregular density structures resembling honeycomb-shaped

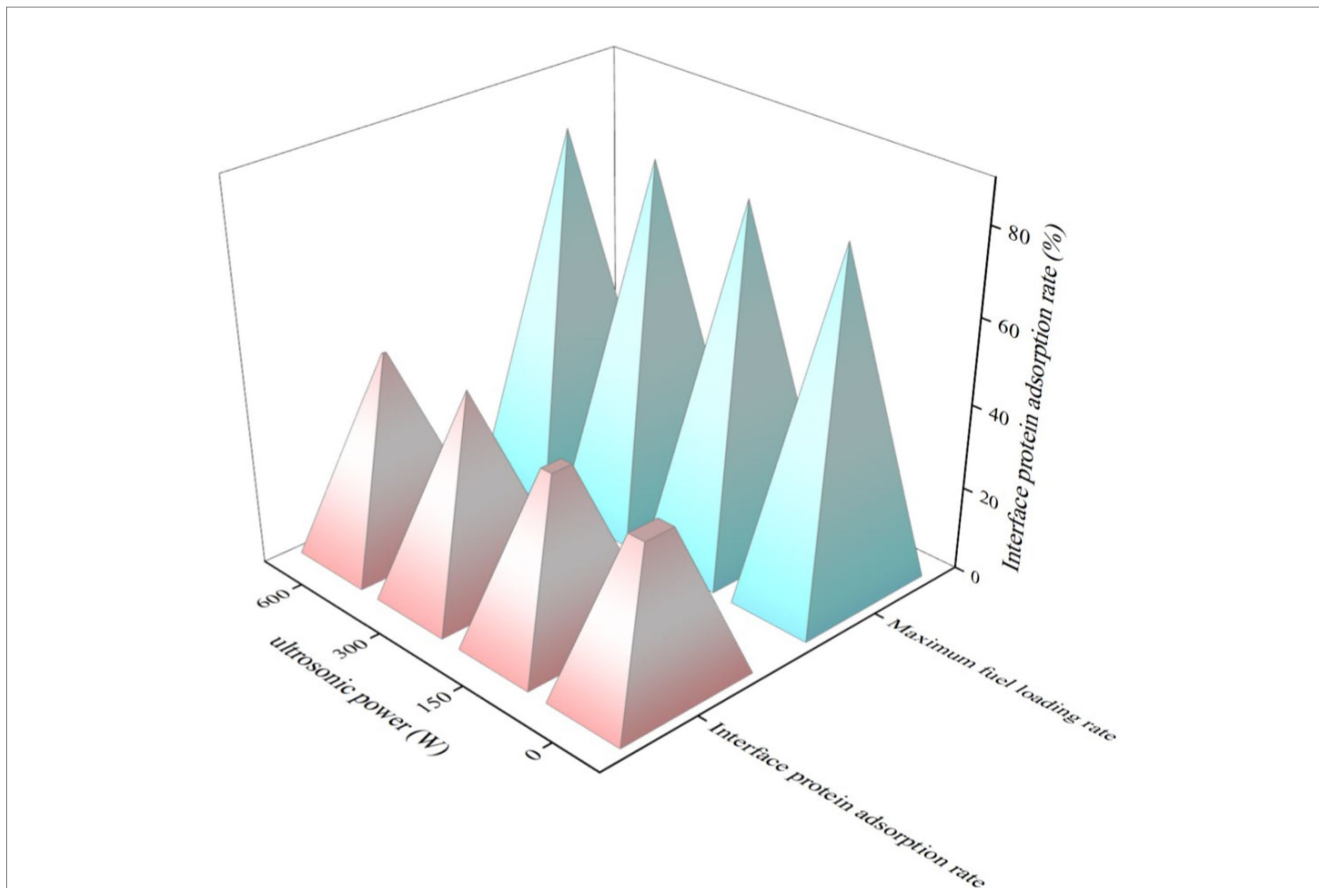


FIGURE 8 Effect of UAPI on the adsorption of stabilized proteins in UAPI-HIPPE and the ratio of HIPPE oil phases (API concentration of 20 mg/mL, pH 2.5).

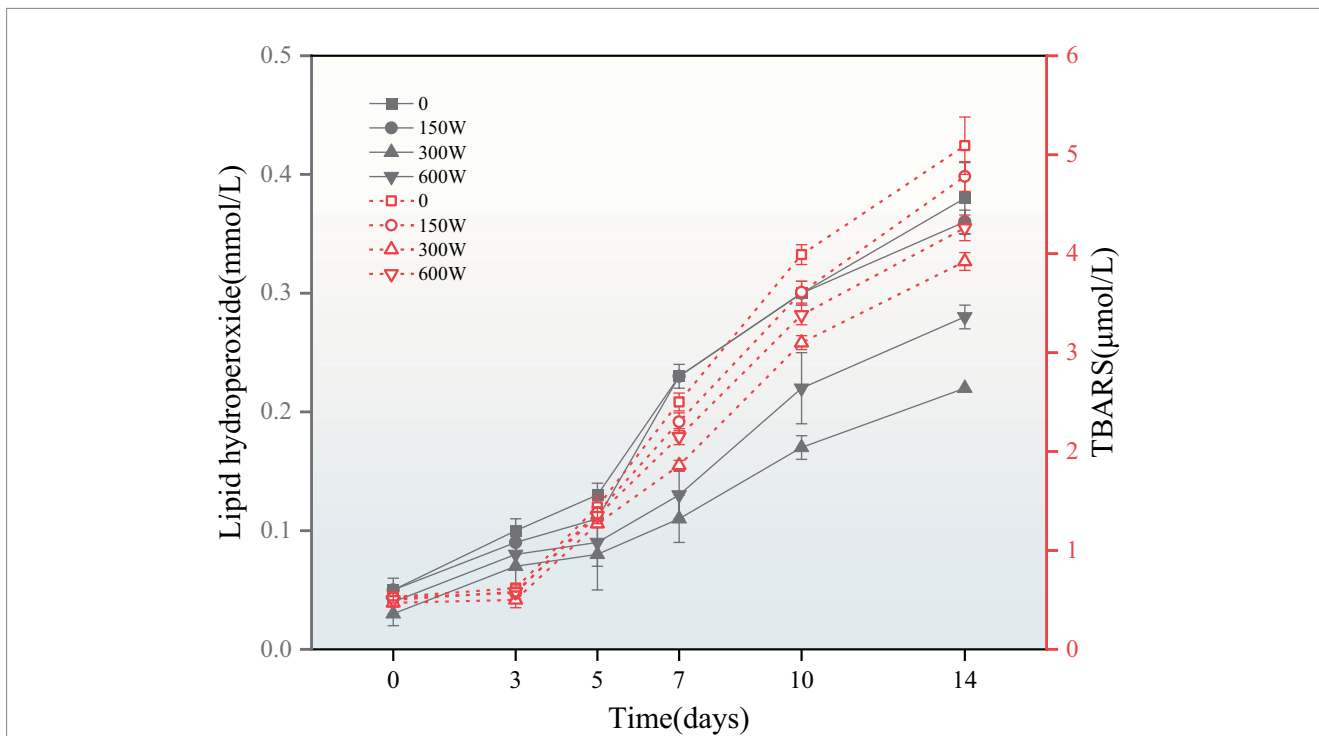


FIGURE 9 The evolution of lipid hydroperoxides and TBARS in UAPI-HIPPEs accelerated their storage at 37°C for 14 days.

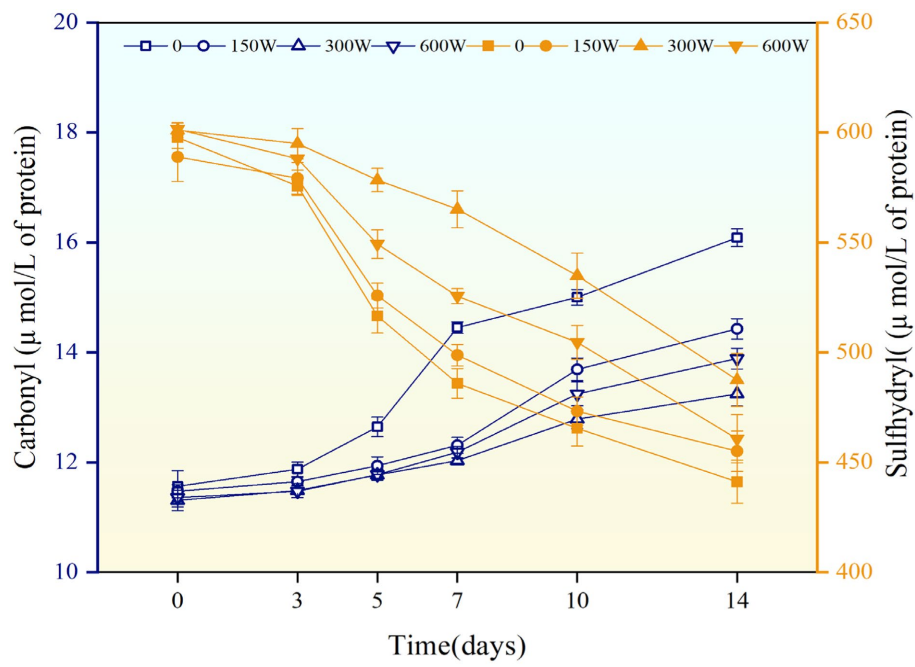


FIGURE 10 The evolution of carbonyl and sulfhydryl groups in UAPI-HIPPES accelerated their storage at 37°C for 14 days.

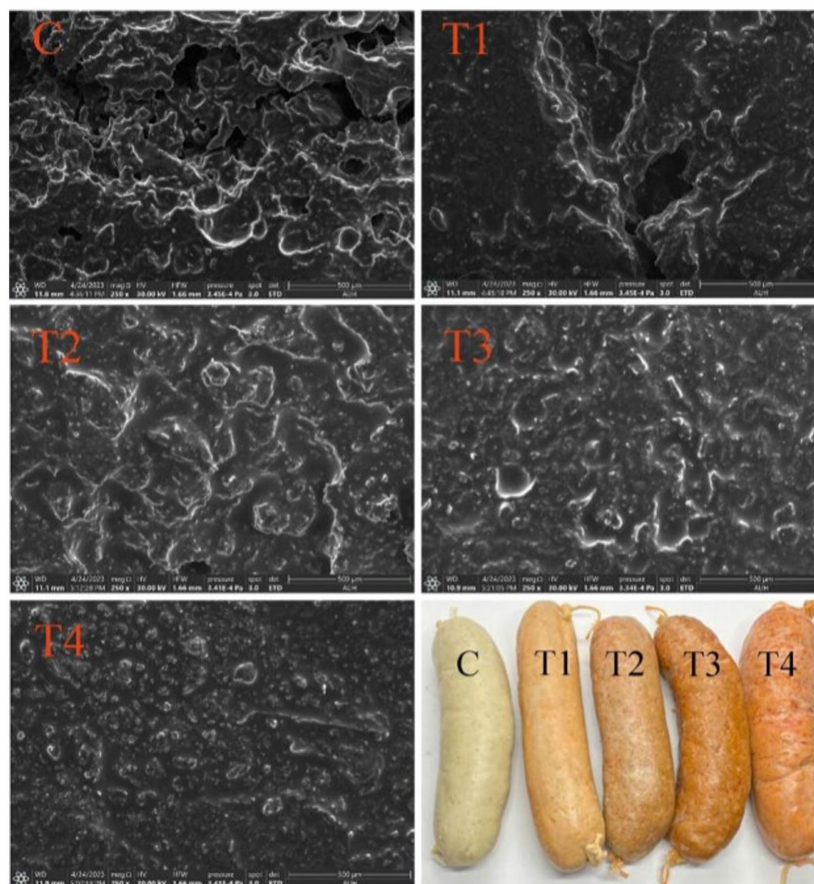


FIGURE 11 Effect of the substitution ratio of UAPI- HIPPES on the microstructure of sausages.

sponges. The formation of these irregular voids can be attributed to the expansion of specific components, predominantly oil, water, and air. Voids could have been generated by the evaporation of water within the sausages during the freeze-drying process (Pires et al., 2020). As the ratio of UAPI-HIPPE increased, the density of the sausage increased, and the three-dimensional network structure lost its honeycomb-spongy structure and became homogeneous. The structural pores of the sausage in the T3 group and T4 group almost disappeared, resulting in a more delicate and smoother structure, presumably due to the even dispersion of fat substitutes in the minced meat during chopping and heating and the formation of an emulsion gel that filled the voids. It has been reported that the use of modified soy protein to prepare high-internal-phase emulsions in sausages resulted in a greater force with an increased amount of emulsion. This was because the emulsion and minced meat bonded tightly and the voids became smaller. The external force of the chopping process and the interaction between the emulsion and minced meat increased, promoting the uniform dispersion of high internal phase emulsions in minced meat (Dickinson, 2019). These results align with this study. Andrés reached the same conclusion, demonstrating that the incorporation of whey protein-stabilized emulsions into low-fat chicken sausages resulted in enhanced microstructure through cross-linking (Andrés et al., 2009). Furthermore, when HIPPEs and minced meat were combined, smaller oil droplets were more uniformly distributed and more readily embedded in the protein matrix than animal fat droplets (Youssef and Barbut, 2011). Moreover, the smaller oil droplets possess a larger surface area, facilitating enhanced interactions between the interfacial nano and the muscle protein matrix.

3.3.2 Cooking loss of sausages

The extent of cooking loss is contingent upon the capacity of minced meat to bind and retain moisture. The magnitude of this phenomenon correlates with the ability of minced meat to bind moisture and fat during heating. As illustrated in Figure 12, the cooking loss of sausages was markedly diminished ($p < 0.05$) with an increase in the substitution ratio of UAPI-HIPPE from 25 to 100%. Compared to the control, the cooking loss of sausages in the T4 group was reduced by 26.48%, indicating that UAPI-HIPPE exhibited superior water-holding capacity during the heating process. As evidenced by the textural properties of the sausages in Table 3, UAPI-HIPPE enhanced the network gel structure of minced meat, facilitating water conservation. Chen et al. (2024) demonstrated that salmon protein proanthocyanidin complex (SPP) stabilized HIPPE replacing the fat in sausages exhibited optimal textural properties and the cooking loss was reduced by 67%.

3.3.3 Texture parameters of sausages

Textural parameters can be used as objective criteria for the evaluation of the overall quality of food products, and are of particular significance as indicators for the assessment of the quality and acceptability of meat products. As illustrated in Table 3, the hardness, chewiness, and cohesiveness of the sausages exhibited a gradual increase with an elevated ratio of UAPI-HIPPE substitution compared with the control ($p < 0.05$). Compared to animal fat (the fat particle size of pig backfat is usually between 10 and 25 millimeters), the particle size of UAPI-HIPPE is considerably smaller (the particle size of 300 W-UAPI-HIPPE is 30.49 μm), which enables effective filling of the three-dimensional gel network matrix of meat protein, resulting

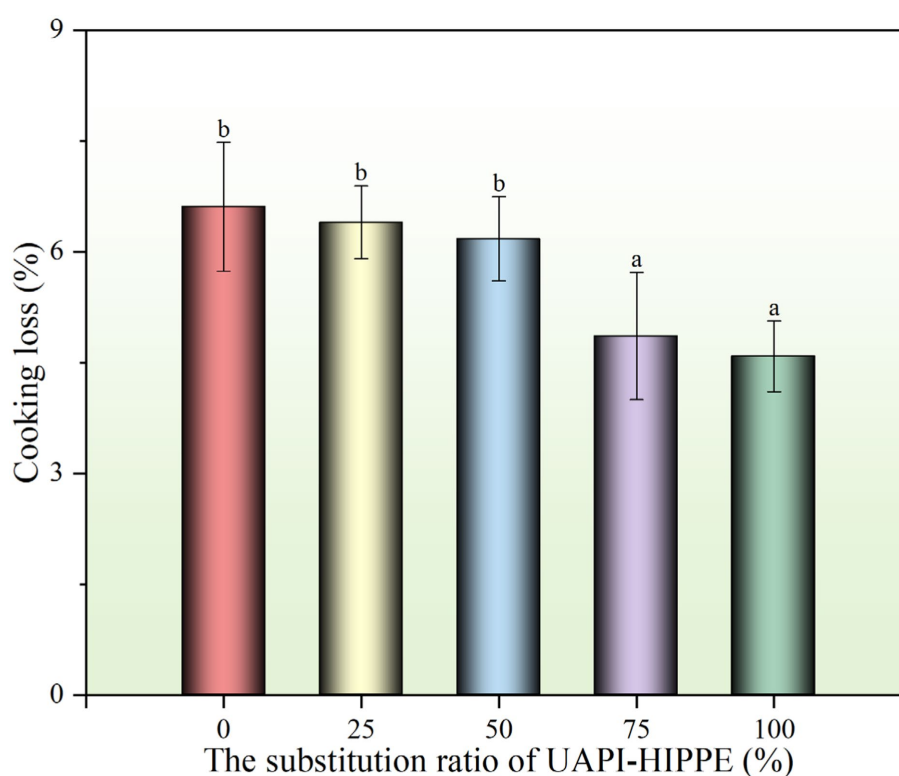


FIGURE 12
Effect of the substitution ratio of UAPI-HIPPEs on cooking loss in sausages.

TABLE 3 Effect of substitution ratio of UAPI-HIPPE on textural parameters of sausages.

Treatment group	Hardness (N)	Resilience (mm)	Chewiness (N·mm)	Cohesiveness (ratio)	Springiness (N·mm)
C	5689.01 ± 1.00 ^a	7.08 ± 0.03 ^a	269.80 ± 1.19 ^a	0.57 ± 0.01 ^a	0.78 ± 0.01 ^a
T1	5797.34 ± 1.20 ^{ab}	7.15 ± 0.02 ^b	284.42 ± 3.66 ^b	0.57 ± 0.01 ^a	0.81 ± 0.02 ^b
T2	5930.21 ± 1.65 ^b	7.16 ± 0.03 ^b	301.50 ± 2.82 ^c	0.59 ± 0.01 ^b	0.86 ± 0.02 ^c
T3	6180.12 ± 1.87 ^c	7.29 ± 0.03 ^c	339.64 ± 1.65 ^d	0.60 ± 0.01 ^c	0.88 ± 0.02 ^c
T4	6216.22 ± 1.97 ^c	7.40 ± 0.02 ^d	345.55 ± 2.42 ^c	0.63 ± 0.01 ^d	0.91 ± 0.01 ^c

Letters a–e following numbers in the same column indicate significant differences between the treatment groups ($p < 0.05$).

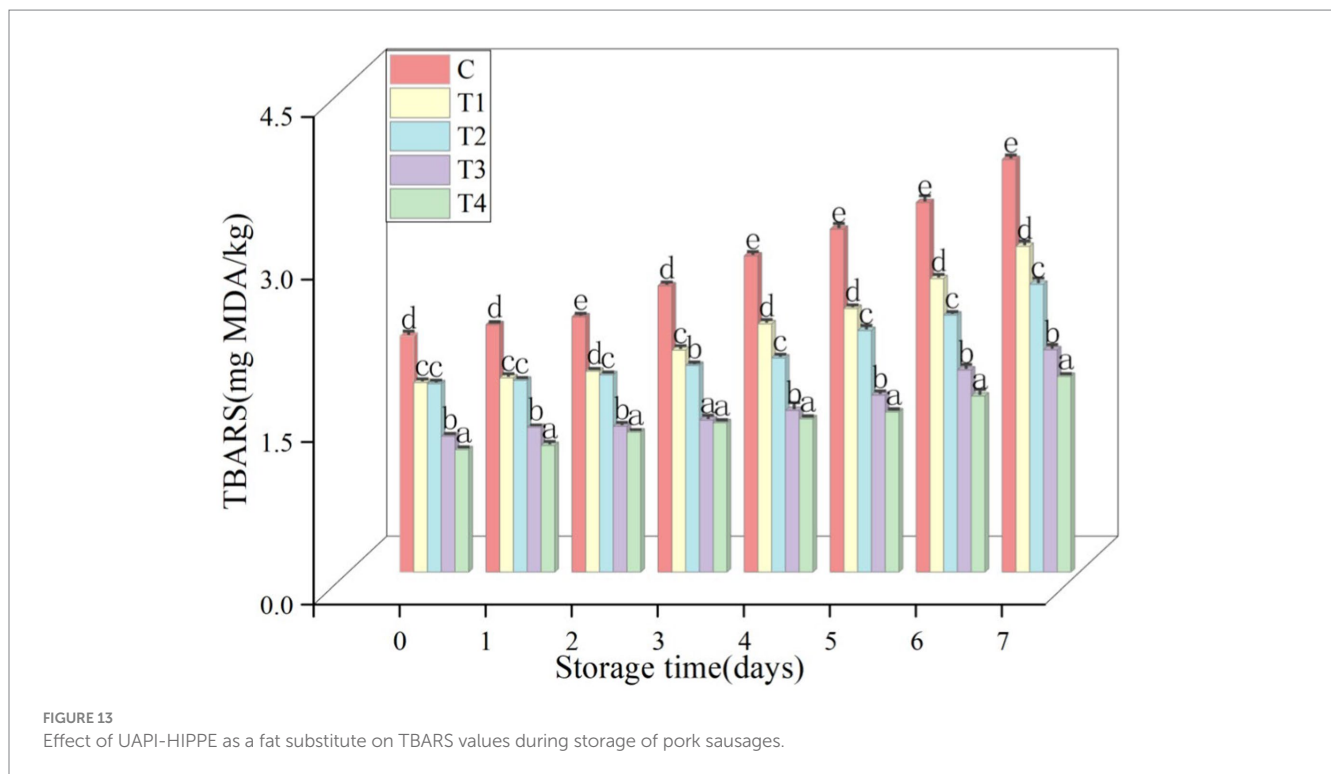


FIGURE 13 Effect of UAPI-HIPPE as a fat substitute on TBARS values during storage of pork sausages.

in relatively high hardness values and chewiness of fat-substituted steamed sausages and enhancement of the mechanical properties of sausages (Paglarini et al., 2019). Similarly, Li et al. used modified pea protein-chitosan complexes as animal fat substitutes, yielding analogous outcomes. This further corroborates the notion that emulsion gel-like animal fat substitutes can impart enhanced hardness to the product (Li et al., 2023). Zhuang et al. discovered that fat substitutes can augment meat gels by facilitating a greater number of protein-protein interactions during cooking, which ultimately results in enhanced hardness (Zhuang et al., 2016). Wang et al. reported that during sausage preparation, heating-induced unfolding of the protein structure leads to the exposure of reactive groups, which promotes protein-muscle protein interactions in the emulsion and the formation of a good network gel structure (Zhou et al., 2012).

3.3.4 TBARS value of sausages

The TBARS content of the sausages stored at 4°C was recorded and is shown in Figure 13. The TBARS content of ready-made sausages exhibited a notable decline ($p < 0.05$) with increasing UAPI-HIPPE concentrations. The TBARS content of each sample gradually increased with prolonged storage time. However, the TBARS content in the alternative group was significantly lower than that in the

control group ($p < 0.05$). Furthermore, the TBARS content of sausages containing 100% UAPI-HIPPE on the seventh day of storage was lower than freshly prepared back fat sausages on the first day, indicating that UAPI-HIPPE exerted a pronounced inhibitory effect on fat oxidation. In a study conducted by Li et al., the substitution of Pickering emulsions stabilized with modified pea protein-chitosan composite (75% corn oil vol. fractions) with 25–100% pig back fat on the sausage quality was investigated. The lowest fat oxidation was observed in sausages with 100% back fat replacement ($p < 0.05$) (Li et al., 2023). Wang et al. used enhanced antioxidant capacity in pork patties through the substitution of fat with a resveratrol-loaded MP-CS complex-stabilized Pickering emulsion, resulting in a notable improvement in the oxidative stability of meat patties (Wang et al., 2023). The use of Pickering emulsions instead of animal fat is an effective method for reducing fat oxidation in meat products.

4 Conclusion

In summary, a Pickering emulsion (75% soybean oil v/v) stabilized by ultrasonically modified API particles was successfully used as a substitute for pork fat without destroying the textural

properties of the sausage. The results of this study confirm that ultrasonication is an effective technique for the preparation of particles with enhanced antioxidant activity and that ultrasonic power has a significant effect on the particle size and interfacial adsorption properties of API. Stable high internal phase emulsions (up to 89% internal phase) could be prepared with UAPI. In addition, API was effectively adsorbed and anchored at the oil–water interface, preventing agglomeration. The UAPI-HIPPE fluid had viscoelastic properties and a pseudo-solid appearance. The addition of Pickering emulsion to sausage induced less cooking loss and fat oxidation and improved the viscoelastic response and texture properties. Overall, UAPI-HIPPE is an ideal material for the replacement of animal fats; these results provide a theoretical basis for the development of sustainable and healthier meat products.

Data availability statement

The original contributions presented in the study are included in the article/supplementary material, further inquiries can be directed to the corresponding authors.

Author contributions

QY: Conceptualization, Data curation, Formal analysis, Investigation, Methodology, Resources, Validation, Writing – original draft. PH: Writing – original draft, Writing – review & editing. WQ: Funding acquisition, Writing – review & editing. YS: Visualization, Writing – original draft. XZ: Data curation, Writing – original draft. FW: Writing – review & editing. ZZ: Conceptualization, Funding acquisition, Project administration, Writing – original draft.

References

- Abdullah, W. J., Ahmad, T., Zhang, C., and Zhang, H. (2020). A review of recent progress on high internal-phase Pickering emulsions in food science. *Trends Food Sci. Technol.* 106, 91–103. doi: 10.1016/j.tifs.2020.10.016
- Andres, S. C., Zaritzky, N. E., and Califano, A. N. (2009). Innovations in the development of healthier chicken sausages formulated with different lipid sources. *Poult. Sci.* 88, 1755–1764. doi: 10.3382/ps.2008-00495
- Asif, M. N., Imran, M., Ahmad, M. H., Khan, M. K., and Hailu, G. G. (2024). Physicochemical and functional properties of *Moringa* seed protein treated with ultrasound. *ACS Omega* 9, 4102–4110. doi: 10.1021/acsomega.3c09323
- Barth, A. (2007). Infrared spectroscopy of proteins. *Biochim. Biophys. Acta Bioenerg.* 1767, 1073–1101. doi: 10.1016/j.bbabi.2007.06.004
- Berton, C., Ropers, M.-H., Guibert, D., Sole, V., and Genot, C. (2012). Modifications of interfacial proteins in oil-in-water emulsions prior to and during lipid oxidation. *J. Agric. Food Chem.* 60, 8659–8671. doi: 10.1021/jf300490w
- Cao, H. W., Sun, R. L., Shi, J. R., Li, M. Y., Guan, X., Liu, J., et al. (2021). Effect of ultrasonic on the structure and quality characteristics of quinoa protein oxidation aggregates. *Ultrason. Sonochem.* 77:105685. doi: 10.1016/j.ulsonch.2021.105685
- Chelch, I., Gatellier, P., and Sante-Lhoutellier, V. (2006). Technical note: a simplified procedure for myofibril hydrophobicity determination. *Meat Sci.* 74, 681–683. doi: 10.1016/j.meatsci.2006.05.019
- Chen, X. T., Huang, J. R., Chen, L. L., Chen, X. N., Su, D. X., and Jin, B. (2023). High internal phase Pickering emulsions stabilised by ultrasound-induced soy protein-beta-glucan-catechin complex nanoparticles to enhance the stability and bioaccessibility of curcumin. *J. Microencapsul.* 40, 456–474. doi: 10.1080/02652048.2023.2220387
- Chen, E. T., Wang, K. Y., Fei, S. Y., Tan, M. Q., and Cheng, S. S. (2024). High internal phase Pickering emulsion with DHA-algal oil stabilized by salmon protein-procyanidin complex and its application in sausages as fat replacer. *Food Biosci.* 58:103702. doi: 10.1016/j.fbio.2024.103702
- Chen, L., and Zhang, S. B. (2023). Structural and functional properties of self-assembled peanut protein nanoparticles prepared by ultrasonic treatment: effects of ultrasound intensity and protein concentration. *Food Chem.* 413:135626. doi: 10.1016/j.foodchem.2023.135626
- Chen, Q. H., Zheng, J., Xu, Y. T., Yin, S. W., Liu, F., and Tang, C. H. (2018). Surface modification improves fabrication of Pickering high internal phase emulsions stabilized by cellulose nanocrystals. *Food Hydrocoll.* 75, 125–130. doi: 10.1016/j.foodhyd.2017.09.005
- Choe, J. H., Kim, H. Y., Lee, J. M., Kim, Y. J., and Kim, C. J. (2013). Quality of frankfurter-type sausages with added pig skin and wheat fiber mixture as fat replacers. *Meat Sci.* 93, 849–854. doi: 10.1016/j.meatsci.2012.11.054
- Deng, X. R., Ma, Y. G., Lei, Y. D., Zhu, X. R., Zhang, L. F., Hu, L., et al. (2021). Ultrasonic structural modification of myofibrillar proteins from *Coregonus peled* improves emulsification properties. *Ultrason. Sonochem.* 76:105659. doi: 10.1016/j.ulsonch.2021.105659
- Dickinson, E. (2019). Strategies to control and inhibit the flocculation of protein-stabilized oil-in-water emulsions. *Food Hydrocoll.* 96, 209–223. doi: 10.1016/j.foodhyd.2019.05.021
- Gulseren, I., Guezey, D., Bruce, B. D., and Weiss, J. (2007). Structural and functional changes in ultrasonicated bovine serum albumin solutions. *Ultrason. Sonochem.* 14, 173–183. doi: 10.1016/j.ulsonch.2005.07.006
- Gumus, C. E., Decker, E. A., and McClements, D. J. (2017). Impact of legume protein type and location on lipid oxidation in fish oil-in-water emulsions: lentil, pea, and faba bean proteins. *Food Res. Int.* 100, 175–185. doi: 10.1016/j.foodres.2017.08.029
- Herrero, A. M. (2008). Raman spectroscopy for monitoring protein structure in muscle food systems. *Crit. Rev. Food Sci. Nutr.* 48, 512–523. doi: 10.1080/10408390701537385

Funding

The author(s) declare that financial support was received for the research, authorship, and/or publication of this article. This work was supported by the Natural Science Foundation of Hebei Province (C2023204010), Sheep System Product Processing and Brand Position (HBCT2024250205), the Research Foundation for the Introduced Talents of Hebei Agricultural University (YJ2021025), and the Hebei Baifeng Agricultural Science and Technology Park Construction (2311N002).

Conflict of interest

The authors declare that the research was conducted in the absence of any commercial or financial relationships that could be construed as a potential conflict of interest.

Generative AI statement

The authors declare that no Gen AI was used in the creation of this manuscript.

Publisher's note

All claims expressed in this article are solely those of the authors and do not necessarily represent those of their affiliated organizations, or those of the publisher, the editors and the reviewers. Any product that may be evaluated in this article, or claim that may be made by its manufacturer, is not guaranteed or endorsed by the publisher.

- Hu, H., Fan, X., Zhou, Z., Xu, X., Fan, G., Wang, L., et al. (2013). Acid-induced gelation behavior of soybean protein isolate with high intensity ultrasonic pre-treatments. *Ultrason. Sonochem.* 20, 187–195. doi: 10.1016/j.ultsonch.2012.07.011
- Ji, J., Zhang, J. P., Chen, J. S., Wang, Y. L., Dong, N., Hu, C. L., et al. (2015). Preparation and stabilization of emulsions stabilized by mixed sodium caseinate and soy protein isolate. *Food Hydrocoll.* 51, 156–165. doi: 10.1016/j.foodhyd.2015.05.013
- Jia, N., Wang, L., Shao, J., Liu, D., and Kong, B. (2017). Changes in the structural and gel properties of pork myofibrillar protein induced by catechin modification. *Meat Sci.* 127, 45–50. doi: 10.1016/j.meatsci.2017.01.004
- Jiang, H. R., Wang, X. Y., Han, L. S., Tang, C. J., He, J., and Min, D. Y. (2023). Intestine-targeted high internal phase Pickering emulsion formulated using silkworm pupa protein via ultrasonic treatment. *Int. J. Biol. Macromol.* 246:125620. doi: 10.1016/j.ijbiomac.2023.125620
- Jiao, B., Shi, A. M., Wang, Q., and Binks, B. P. (2018). High-internal-phase Pickering emulsions stabilized solely by Peanut-protein-isolate microgel particles with multiple potential applications. *Angew. Chem. Int. Ed Engl.* 57, 9274–9278. doi: 10.1002/anie.201801350
- Joshi, R., Sood, S., Dogra, P., Mahendru, M., Kumar, D., Bhangalia, S., et al. (2013). *In vitro* cytotoxicity, antimicrobial, and metal-chelating activity of triterpene saponins from tea seed grown in Kangra valley, India. *Med. Chem. Res.* 22, 4030–4038. doi: 10.1007/s00044-012-0404-4
- Keramat, M., Kheynoor, N., and Golmakani, M. T. (2022). Oxidative stability of Pickering emulsions. *Food Chem. X* 14:100279. doi: 10.1016/j.fochx.2022.100279
- Li, J., Dai, Z., Chen, Z., Hao, Y., Wang, S., and Mao, X. (2023). Improved gelling and emulsifying properties of myofibrillar protein from frozen shrimp (*Litopenaeus vannamei*) by high-intensity ultrasound. *Food Hydrocoll.* 135:108188. doi: 10.1016/j.foodhyd.2022.108188
- Li, K., Liu, J. Y., Fu, L., Zhao, Y. Y., and Bai, Y. H. (2019). Comparative study of thermal gelation properties and molecular forces of actomyosin extracted from normal and pale, soft and exudative-like chicken breast meat. *Asian Australas. J. Anim. Sci.* 32, 721–733. doi: 10.5713/ajas.18.0389
- Li, N., Wang, T., Yang, X. R., Qu, J. Y., Wang, N., Wang, L. Q., et al. (2022). Effect of high-intensity ultrasonic treatment on the emulsion of hemp seed oil stabilized with hemp seed protein. *Ultrason. Sonochem.* 86:106021. doi: 10.1016/j.ultsonch.2022.106021
- Li, C. Q., Xie, W. R., Zhang, X., Liu, J., Zhang, M. Y., and Shao, J. H. (2023). Pickering emulsion stabilized by modified pea protein-chitosan composite particles as a new fat substitute improves the quality of pork sausages. *Meat Sci.* 197:109086. doi: 10.1016/j.meatsci.2022.109086
- Li, R. N., and Xiong, Y. L. (2021). Ultrasound-induced structural modification and thermal properties of oat protein. *LWT Food Sci. Technol.* 149:111861. doi: 10.1016/j.lwt.2021.111861
- Luo, Q. Y., Li, X. M., Zhang, Z. Q., Chen, A. J., Li, S. S., Shen, G. H., et al. (2022). Extraction of Zanthoxylum seed protein and identification of its simulated digestion products. *LWT Food Sci. Technol.* 161:113412. doi: 10.1016/j.lwt.2022.113412
- Ma, W. C., Wang, J. M., Xu, X. B., Qin, L., Wu, C., and Du, M. (2019). Ultrasound treatment improved the physicochemical characteristics of cod protein and enhanced the stability of oil-in-water emulsion. *Food Res. Int.* 121, 247–256. doi: 10.1016/j.foodres.2019.03.024
- Mandalari, G., Tomaino, A., Arcoraci, T., Martorana, M., Lo Turco, V., Cacciola, F., et al. (2010). Characterization of polyphenols, lipids and dietary fibre from almond skins (*Amygdalus communis* L.). *J. Food Compos. Anal.* 23, 166–174. doi: 10.1016/j.jfca.2009.08.015
- Marquez, A. L., Medrano, A., Panizzolo, L. A., and Wagner, J. R. (2010). Effect of calcium salts and surfactant concentration on the stability of water-in-oil (w/o) emulsions prepared with polyglycerol polyricinoleate. *J. Colloid Interface Sci.* 341, 101–108. doi: 10.1016/j.jcis.2009.09.020
- Martinez, I., Sanchez-Alonso, I., Pineiro, C., Careche, M., and Carrera, M. (2020). Protein signatures to trace seafood contamination and processing. *Food Secur.* 9:1751. doi: 10.3390/foods9121751
- Morales, R., Martinez, K. D., Pizonas Ruiz-Henestrosa, V. M., and Pilosof, A. M. R. (2015). Modification of foaming properties of soy protein isolate with high ultrasound intensity: particle size effect. *Ultrason. Sonochem.* 26, 48–55. doi: 10.1016/j.ultsonch.2015.01.011
- Oliete, B., Potin, F., Cases, E., and Saurel, R. (2018). Modulation of the emulsifying properties of pea globulin soluble aggregates by dynamic high-pressure fluidization. *Innovative Food Sci. Emerg. Technol.* 47, 292–300. doi: 10.1016/j.ifset.2018.03.015
- Paglarini, C. S., Furtado, G. F., Honorio, A. R., Mokarze, L., da Silva Vidal, V. A., Badan Ribeiro, A. P., et al. (2019). Functional emulsion gels as pork back fat replacers in Bologna sausage. *Food Struct. Netherlands* 20:100105. doi: 10.1016/j.foosr.2019.100105
- Peng, W. W., Kong, X. Z., Chen, Y. M., Zhang, C. M., Yang, Y. X., and Hua, Y. F. (2016). Effects of heat treatment on the emulsifying properties of pea proteins. *Food Hydrocoll.* 52, 301–310. doi: 10.1016/j.foodhyd.2015.06.025
- Pires, M. A., Barros, J. C., Rodrigues, I., Munekata, P. E. S., and Trindade, M. A. (2020). Improving the lipid profile of bologna type sausages with Echium (*Echium plantagineum* L.) oil and chia (*Salvia hispanica* L.) flour. *LWT Food Sci. Technol.* 119:108907. doi: 10.1016/j.lwt.2019.108907
- Qayam, A., Li, M., Shi, R. J., Bilawal, A., Gantumur, M. A., Hussain, M., et al. (2021). Laccase cross-linking of sonicated α -Lactalbumin improves physical and oxidative stability of CLA oil in water emulsion. *Ultrason. Sonochem.* 71:105365. doi: 10.1016/j.ultsonch.2020.105365
- Qin, X. S., Luo, Z. G., and Peng, X. C. (2018). Fabrication and characterization of quinoa protein nanoparticle-stabilized food-grade Pickering emulsions with ultrasound treatment: interfacial adsorption/arrangement properties. *J. Agric. Food Chem.* 66, 4449–4457. doi: 10.1021/acs.jafc.8b00225
- Rahman, M. M., and Lamsal, B. P. (2021). Ultrasound-assisted extraction and modification of plant-based proteins: impact on physicochemical, functional, and nutritional properties. *Compr. Rev. Food Sci. Food Saf.* 20, 1457–1480. doi: 10.1111/1541-4337.12709
- Schroen, K., and Berton-Carabin, C. C. (2022). A unifying approach to lipid oxidation in emulsions: modelling and experimental validation. *Food Res. Int.* 160:111621. doi: 10.1016/j.foodres.2022.111621
- Shantha, N. C., and Decker, E. A. (1994). Rapid, sensitive, iron-based spectrophotometric methods for determination of peroxide values of food. *LIPIDS J. AOAC Int.* 77, 421–424. doi: 10.1093/jaoac/77.2.421
- Shi, A. M., Feng, X. Y., Wang, Q., and Adhikari, B. (2020). Pickering and high internal phase Pickering emulsions stabilized by protein-based particles: a review of synthesis, application and prospective. *Food Hydrocoll.* 109:106117. doi: 10.1016/j.foodhyd.2020.106117
- Sun, X. H., Sarteshnizi, R. A., and Udenigwe, C. C. (2022). Recent advances in protein-polyphenol interactions focusing on structural properties related to antioxidant activities. *Curr. Opin. Food Sci.* 45:100840. doi: 10.1016/j.cofs.2022.100840
- Sun, Y., Yu, X. X., Hussain, M., Li, X. D., Liu, L., Liu, Y. B., et al. (2022). Influence of ultrasound treatment on the morphological characteristics, structures and emulsifying properties of mimicking human fat emulsions. *Ultrason. Sonochem.* 82:105881. doi: 10.1016/j.ultsonch.2021.105881
- Tao, Y., Wang, P., Xu, X. L., Chen, J. H., Huang, M. Y., and Zhang, W. Y. (2023). Effects of ultrasound treatment on the morphological characteristics, structures and emulsifying properties of genipin cross-linked myofibrillar protein. *Ultrason. Sonochem.* 97:106467. doi: 10.1016/j.ultsonch.2023.106467
- Tian, R., Feng, J. R., Huang, G., Tian, B., Zhang, Y., Jiang, L. Z., et al. (2020). Ultrasound driven conformational and physicochemical changes of soy protein hydrolysates. *Ultrason. Sonochem.* 68:105202. doi: 10.1016/j.ultsonch.2020.105202
- Villa, C., Moura, M., Costa, J., and Mafra, I. (2022). β -Lactoglobulin versus casein indirect ELISA for the detection of cow's milk allergens in raw and processed model meat products. *Food Control* 135:108818. doi: 10.1016/j.foodcont.2022.108818
- Wang, M. R., Ma, L., Xie, P., Li, C. P., Yang, X. X., and Lang, Y. M. (2023). Improved antioxidant properties of pork patties by replacing fat with resveratrol-loaded MP-CS complex stabilized Pickering emulsion. *Food Sci. Technol. Int.* 10820132231196202. doi: 10.1177/10820132231196202
- Wang, L. L., and Xiong, Y. L. (2005). Inhibition of lipid oxidation in cooked beef patties by hydrolyzed potato protein is related to its reducing and radical scavenging ability. *J. Agric. Food Chem.* 53, 9186–9192. doi: 10.1021/jf051213g
- Xia, M. Q., Chen, Y. X., Guo, J. J., Huang, H., Wang, L., Wu, W. J., et al. (2019). Water distribution and textural properties of heat-induced pork myofibrillar protein gel as affected by sarcoplasmic protein. *LWT Food Sci. Technol.* 103, 308–315. doi: 10.1016/j.lwt.2019.01.009
- Yan, S. Z., Xu, J. W., Zhang, S., and Li, Y. (2021). Effects of flexibility and surface hydrophobicity on emulsifying properties: ultrasound-treated soybean protein isolate. *LWT Food Sci. Technol.* 142:110881. doi: 10.1016/j.lwt.2021.110881
- Youssef, M. K., and Barbut, S. (2011). Fat reduction in comminuted meat products-effects of beef fat, regular and pre-emulsified canola oil. *Meat Sci.* 87, 356–360. doi: 10.1016/j.meatsci.2010.11.011
- Zhang, X., Liang, H. S., Li, J., Wei, X. L., and Li, B. (2020). Improving the emulsifying property of gliadin nanoparticles as stabilizer of Pickering emulsions: modification with sodium carboxymethyl cellulose. *Food Hydrocoll.* 107:105936. doi: 10.1016/j.foodhyd.2020.105936
- Zhang, X. X., Zuo, Z. Y., Ma, W. J., Yu, P. B., Li, T., and Wang, L. (2021). Assemble behavior of ultrasound-induced quinoa protein nanoparticles and their roles on rheological properties and stability of high internal phase emulsions. *Food Hydrocoll.* 117:106748. doi: 10.1016/j.foodhyd.2021.106748
- Zhang, X. X., Zuo, Z. Y., Yu, P. B., Li, T., Guang, M., Chen, Z. X., et al. (2021). Rice peptide nanoparticle as a bifunctional food-grade Pickering stabilizer prepared by ultrasonication: structural characteristics, antioxidant activity, and emulsifying properties. *Food Chem.* 343:128545. doi: 10.1016/j.foodchem.2020.128545
- Zhou, C., Wang, J., Wang, H., Zhang, L., and Cai, K. (2012). Effect of Carboxy-hemoglobin on color stability of cooked pork sausage. *Food Sci. Biotechnol.* 21, 267–272. doi: 10.1007/s10068-012-0035-z
- Zhou, L., Zhang, J., Xing, L. J., and Zhang, W. G. (2021). Applications and effects of ultrasound assisted emulsification in the production of food emulsions: a review. *Trends Food Sci. Technol.* 110, 493–512. doi: 10.1016/j.tifs.2021.02.008
- Zhu, Q. Q., Chen, W. X., Wang, L. C., Chen, W. J., Zhang, M., Zhong, Q. P., et al. (2024). Development of high internal phase emulsions using coconut protein isolates modified by pulsed light: relationship of interfacial behavior and emulsifying stability. *Food Hydrocoll.* 148:109495. doi: 10.1016/j.foodhyd.2023.109495
- Zhuang, X., Han, M., Kang, Z.-l., Wang, K., Bai, Y., Xu, X.-l., et al. (2016). Effects of the sugarcane dietary fiber and pre-emulsified sesame oil on low-fat meat batter physicochemical property, texture, and microstructure. *Meat Sci.* 113, 107–115. doi: 10.1016/j.meatsci.2015.11.007